Nano Research 2017, 10(6): 1872–1879
DOI 10.1007/s12274-016-1369-2
Research Article

ISSN 1998-0124
CN 11-5974/O4

Broadband photovoltaic effect of n-type topological insulator Bi_2Te_3 films on p-type Si substrates

Zhenhua Wang[1,2], Mingze Li[1,2], Liang Yang[1,2], Zhidong Zhang[1,2] (✉), and Xuan P. A. Gao[3] (✉)

[1] *Shenyang National Laboratory for Materials Science, Institute of Metal Research, Chinese Academy of Sciences, 72 Wenhua Road, Shenyang 110016, China*
[2] *School of Materials Science and Engineering, University of Science and Technology of China, 96 Jinzhai Road, Hefei 230026, China*
[3] *Department of Physics, Case Western Reserve University, Cleveland, Ohio 44106, USA*

Received: 11 July 2016
Revised: 10 November 2016
Accepted: 15 November 2016

KEYWORDS

photovoltaic effect,
topological insulators,
Bi_2Te_3/Si,
film

ABSTRACT

We report the photovoltaic effects of n-type topological insulator (TI) Bi_2Te_3 films grown on p-type Si substrates by chemical vapor deposition (CVD). The films containing large nanoplates with a smooth surface formed on p-Si exhibit good p–n diode characteristics under dark and light illumination conditions and display a good photovoltaic effect under the broadband range from ultraviolet (UV) to near infrared (NIR) wavelengths. Under the light illumination with a wavelength of 1,000 nm, a short circuit current (I_{SC}) of 19.2 μA and an open circuit voltage (V_{OC}) of 235 mV are achieved. The maximum fill factor (FF) increases with a decrease in the wavelength or light density, achieving a value of 35.6% under 600 nm illumination. The photoresponse of the n-Bi_2Te_3/p-Si device can be effectively switched between the on and off modes in millisecond time scale. These findings are important for both the fundamental understanding and solar cell device applications of TI materials.

1 Introduction

In a p–n junction solar cell, an electric current is generated on illuminating the material as the excited electrons and remaining holes are swept in different directions by the built-in electric field in the depletion region. This effect, which was initially discovered with silicon and later with gallium arsenide, can be utilized for achieving energy-efficient electronic-photonic integrated circuits [1]. The p- and n-type regions can be formed by chemically doping a bulk semiconductor to create a junction region for a conventional p–n homo-junction. The p–n hetero-junctions can also be realized with the epitaxial growth of an n/p-type semiconductor on another p/n-type semiconductor. In the past few years, the research on two-dimensional (2D) materials has been increasing rapidly, as they are proved to be promising candidates for next generation electronic devices owing to their remarkable mechanical [2], electrical [3], and optical properties [4]. These materials form the basis of the new atomically thin optoelectronic devices such as

Address correspondence to Zhidong Zhang, zdzhang@imr.ac.cn; Xuan P. A. Gao, xuan.gao@case.edu

solar cells and devices used for transistor operation [3, 5], optical communication [6] and photodetection [7, 8]. Graphene and transition metal dichalcogenide (MoS_2, WSe_2, et al.) 2D nanomaterials exhibit a great promise for photonic applications owing to their unique properties associated with their ultrathin planar structures [9, 10]. Graphene can absorb light in a wide range of wavelengths in the visible spectra and generate a photocurrent, thereby serving as an excellent light-to-current converter reaching close to 100% [11]. The photovoltaic effect of graphene-based devices has been demonstrated [12]. The photodetectors based on MoS_2 thin layers have been shown to exhibit a high photo-responsivity, which is higher than that of the graphene-based devices [13]. A photodetector based on graphene/MoS_2 heterostructure exhibiting a high photogain (greater than 10^8) has been demonstrated [14]. P-type WSe_2 and n-type MoS_2 were used to fabricate atomically thin p–n junctions using van der Waals-bonded semiconductor layers. This junction exhibited both rectifying electrical characteristics and a photovoltaic response, for which the extended depletion region played a crucial role [15]. The p-type black phosphorus and n-type monolayer MoS_2 can be used for forming an atomically sharp type II heterointerface through van der Waals interactions [16]. The p–n diode exhibited gate-tunable current-rectifying characteristics. The photovoltaic power generation in the diode resulted in a high external quantum efficiency of ~0.3% [17]. By designing and fabricating MoS_2 monolayers on a p-Si substrate heterojunction solar cell device, the highest efficiency (reaching a power conversion efficiency of 5.23%) reported for a monolayer transition-metal dichalcogenide-based solar cell could be achieved [18]. Different 2D materials can be used as components of a single device such as a photodetector [19] by using a gate dielectric and semiconducting channel material. An ambipolar material is required to create a p–n junction. Recently, electrostatically defined p–n junctions have been fabricated with WSe_2, demonstrating its potential in optoelectronic devices [20, 21]. The photovoltaic and photothermoelectric effects of the double-gated WSe_2 device were examined. When the device was operated in the p–n configuration, the photocurrent was generated mostly due to the photovoltaic effect. When the gates were biased in the p–p configuration, the photocurrent was generated mainly due to the photothermoelectric effect [21]. Recently, a Bi_2Se_3/Si heterostructure was prepared using a physical vapor deposition method, which exhibited a pronounced photodetector response under light illumination [22].

Bi_2Te_3, a chalcogenide with a layered van der Waals crystal structure, is known to act as a three-dimensional (3D) topological insulator (TI) owing to their Dirac surface states as analyzed by angle-resolved photo-electron spectroscopy (ARPES) [23]. The carrier mobility on the Bi_2Te_3 surface was measured to be as high as ~5,000 $cm^2/(V\cdot s)$ [24]. Recently, it was proposed that the simplest 3D TIs could function as a new class of saturable absorbers [25, 26]. Because the Dirac-like linear dispersion band on the surface states of Bi_2Te_3 crystals with a narrow energy bandgap of ~0.17 eV [27], it is expected to exhibit the broadband saturable absorption property. The use of n- and p-type Bi_2Te_3 nanoparticles as nonlinear saturable absorbers was investigated, revealing a broadband saturable absorption at 800 and 1,570 nm [28]. Because of the effective photocarrier generation and transfer at the interface between graphene and Bi_2Te_3, the photocurrent in the graphene-Bi_2Te_3 heterostructure device can be effectively enhanced without sacrificing the detecting spectral width [19]. Nevertheless, Bi_2Te_3 contains vacancies and antisite-based crystalline defects; hence, the as-grown Bi_2Te_3 nanostructures or films exhibit n-type characteristics as shown in our previous studies [29, 30]. Moreover, the ultra-broadband photodetector based on a Bi_2Te_3/Si heterostructure was examined. Bi_2Te_3/Si was prepared using the pulsed laser deposition (PLD) method [31] and the photoresponse of the heterojunction was examined for photodetector applications. The device demonstrated a room-temperature photodetection from the ultraviolet (UV) to terahertz region with a good reproducibility. The time-dependent switching behavior examined at zero bias and –5 V source-drain bias suggested a strong switching behavior achieved with the source-drain bias [31]. Thus, it would be interesting to integrate Bi_2Te_3 with silicon to prepare n-type Bi_2Te_3/p-Si junctions and study the photovoltaic effect of these junctions under light illumination. Due to the broadband absorption property of Bi_2Te_3, an n-Bi_2Te_3/p-Si junction could be a promising candidate for new p–n junction solar cells.

Here, we fabricate n-type TI Bi_2Te_3/p-Si (Si doped with B) junctions and characterize their photovoltaic responses. The formation of the p–n junction is demonstrated by the nonlinear diode type *I*–*V* characteristics of the devices. On measuring the photocurrent (and photovoltage) under light illumination, we find that the photocurrent generation is dominated by the photovoltaic effect in our n-Bi_2Te_3/p-Si junctions. The best device displays short-circuit currents of up to 19.2 μA and open-circuit voltages of up to 235 mV under 1,000 nm wavelength illumination with a light intensity of about 175 W/m^2. The on–off response-time of photocurrent (and photovoltage) under dark and illumination conditions is in the order of milliseconds or shorter. The transport properties and photovoltaic effects are affected by the quality of the p–n junction, which might depend on the morphology of Bi_2Te_3 films. The p–n diode characteristics with a good photovoltaic effect are obtained with the smooth Bi_2Te_3 films formed with large Bi_2Te_3 nanoplates.

2 Experimental

2.1 Preparation of Bi_2Te_3 films

Bi_2Te_3 films were grown using the chemical vapor deposition (CVD) method on Si substrates with a size of ~1.5 cm × 1.5 cm in 10% H_2/Ar carrier gas. Before depositing the Bi_2Te_3 film, the p-type Si substrate was cleaned with ethanol and acetone under ultrasonication for ~5 min followed by immersed it in dilute HF acid (~5%) for ~50 s in order to remove the native oxide layer present on the surface. A high-temperature tube furnace and a quartz tube with a diameter of ~2.5 cm were used for the synthesis by accurately controlling the temperature and gas flow rate. The substrate was placed at a distance of 14–15 cm away from the center of the furnace. Bi_2Te_3 powder with a purity of 99.99% was used as the precursor, which was placed at the center of the furnace at 520 °C. A growth process similar to that reported in our previous study in which a Bi_2Te_3 film was prepared on semi-insulating Si was employed [30]. The structural and morphological analyses of the samples were performed using scanning electron microscopy (SEM), and X-ray diffraction (XRD) was employed to analyze the stoichiometry of Bi_2Te_3. The size of the flakes formed in the Bi_2Te_3 film was controlled by tuning the working pressure. A high pressure (~50 Pa) is favorable for the production of big flakes and a low pressure (~30 Pa) is favorable for the production of small flakes. Rectangle shaped samples with a length of <1 cm and a width of ~2–4 mm were cut from the wafer for performing transport and photovoltaic effect measurements. To fabricate a device, a part of the Bi_2Te_3 film (about 1 mm × ~2–4 mm) was removed in order to reveal the surface of the Si substrate, which was used as one electrode, and the Bi_2Te_3 film was used as the second electrode. Silver paint was used to attach copper wires to the surface of the Bi_2Te_3 film and the exposed Si substrate for conducting electrical measurements.

2.2 Photoresponse measurements

A solar-500 W xenon lamp was used as the light source, which exhibits a continuous energy spectral distribution from 200–1,200 nm. A light intensity of ~250 W/m^2 with a current of ~15 A were used. Filters with different wavelengths were used to obtain a monochromatic light, causing a decrease in the light intensity to ~175 W/m^2. In order to control the intensity of light, additional filters with different optical densities were used.

3 Results and discussion

3.1 Structures of the Bi_2Te_3 films

A CVD process was employed to synthesize n-Bi_2Te_3 films on p-type Si substrates (see Methods section). SEM images of the Bi_2Te_3 films formed on p-Si indicate the uniformity of the films. The samples containing large plates are named as Sample1 and Sample3, which were prepared with a working pressure of ~50 Pa. The samples containing small plates are named as Sample2 and Sample4, which were obtained with a working pressure of ~30 Pa. The typical SEM images of Bi_2Te_3 films corresponding to Sample1 and Sample2 are shown in Figs. 1(a) and 1(b), showing the Bi_2Te_3 nanoplates with different sizes. As shown in the SEM images, the films are formed with interconnected grains of Bi_2Te_3 nanoplates. SEM images showing nanoplates

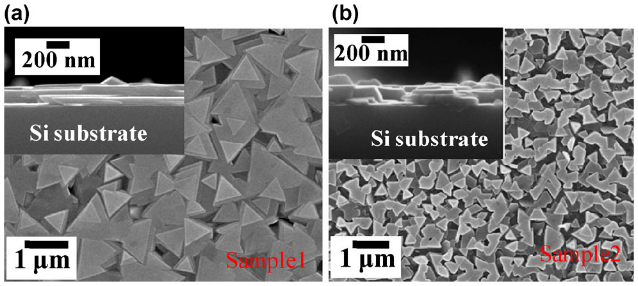

Figure 1 SEM images of the Bi_2Te_3 thin film in the (a) Sample1 containing large nanoplates and (b) Sample2 containing small nanoplates. The side view image of the sample is shown in the inset of (a) and (b).

with different sizes are also given in Figs. S1(a) and S1(b) (in the Electronic Supplementary Material (ESM)). The thickness of the films can be estimated from the side-view SEM images of the samples (SEM images shown in the inset of Figs. 1(a) and 1(b)). The layer thickness of the films is typically about 210 ± 10 nm. All the samples exhibit similar XRD patterns. Figure S1(c) in the ESM shows the XRD pattern of a typical Bi_2Te_3 thin film. The film grows along the *c*-axis orientation, (003n) tropism, in consistent with the SEM images, which indicate that all the flakes lie on the substrate.

3.2 Photoresponse of the Bi_2Te_3/Si films

All the measurements were performed at room temperature and ambient atmosphere. Figure 2(a) shows the schematic of the n-Bi_2Te_3/p-Si photodetector device. The photo-excited carriers are separated by the built-in electric field at the junction between the n-Bi_2Te_3 and p-Si having different work function values. The estimated energy band of Bi_2Te_3/Si indicates that the n-Bi_2Te_3 films and p-Si form a type-II heterojunction with a relatively high built-in field, which might result in excellent photovoltaic performances [31, 32]. The Fermi level of n-Bi_2Te_3 is located above the bottom of the bulk conduction band [19]. For an ideal semiconductor p–n junction, the doping concentration of semiconductors, dielectric permittivity, built-in voltage, and the applied bias affect the depletion condition/width of the p–n junction. For Bi_2Te_3 films grown on a Si substrate, surface defects and interfacial traps are induced, and should be considered in a more comprehensive model [18]. The *I*–*V* characteristics of Sample1 and Sample2 under dark and illumination conditions for different light wavelengths are given in Figs. 2(b) and 2(c). The *I*–*V* characteristics of other samples indicating well-defined diode behaviors are shown in Fig. S2 (in the ESM). The photovoltaic effect observed for the Sample1 confirms that a good p–n junction is formed in the films consisting of large Bi_2Te_3 nanoplates. The rectifying character of the p–n diode is found to weaken under light illumination as shown in Fig. 2(c). This indicates that the built-in potential at the p–n junction of Sample2 is not strong enough, causing photoconductivity to be dominant [33, 34]. Figures 2(d) and 2(e) display the *I*–*V* characteristics of Sample1 and Sample2 for different light densities under illumination with a wavelength of 1,000 nm. The *I*–*V* curves show a typical p–n junction behavior under light illumination for all the densities examined for Sample1. However, the *I*–*V* curves of the Sample2 indicate a rectifying character only under light illumination with a low intensity. The electrical conductivity of the sample increases under high-density light illumination due to the absorption of light as shown in Fig. 2(e). These results confirm that the Sample2 exhibits photoconductivity properties under near infrared (NIR) and high density light illumination conditions.

The typical short-circuit current (I_{SC}, current at zero bias) and open-circuit voltage (V_{OC}, voltage without current flow) values obtained under 1,000 nm illumination are displayed in the inset of Fig. 2(b). Under 1,000 nm light illumination, the highest values of I_{SC} (19.2 μA) and V_{OC} (235 mV) are achieved. The power generated by the p–n diode can be calculated as $P_d = I_d \times V_d$ (Fig. 3(b)). The FF can be calculated as $FF = P_d/(I_{SC} \times V_{OC})$. The maximum value of FF is increased from 30.8% to 35.6% on decreasing the wavelength from 1,000 to 600 nm (as shown in Fig. S3(a) in the ESM). In order to analyze the photovoltaic properties of the Sample1, the I_{SC} and V_{OC} values are extracted from the data given in Figs. 2(b) and 2(d) with respect to the light wavelength and density, which are given in Figs. 3(a) and 3(c), respectively. I_{SC} and V_{OC} initially increase on increasing the light wavelength from 300 to 1,000 nm, and then decrease at higher wavelengths. The enhanced I_{SC} and V_{OC}

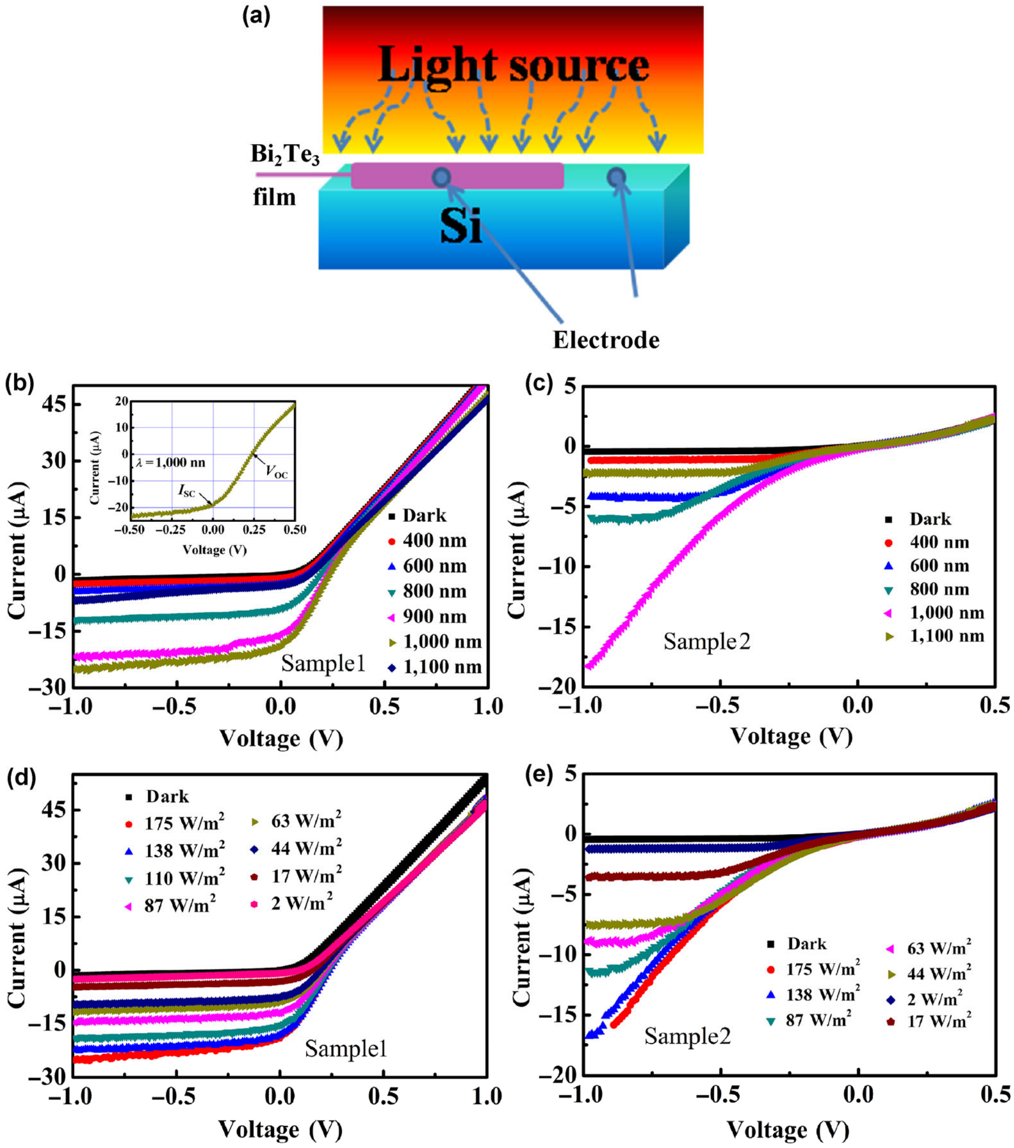

Figure 2 (a) Schematic of the n-Bi_2Te_3/p-Si junction structure. *I*–*V* characteristics of n-Bi_2Te_3/p-Si under dark and illumination conditions with different light wavelengths for (b) Sample1 and (c) Sample2. *I*–*V* characteristics of (d) Sample1 and (e) Sample2 under illumination with different light densities (λ = 1,000 nm).

values are observed at ~900–1,000 nm. The broadband photo-response of the n-Bi_2Te_3/p-Si junction in the UV to NIR wavelength range is demonstrated. The I_{SC} and V_{OC} values increase as the light density increases (Fig. 3(c)). I_{SC} follows a near linear dependence on the light density, whereas V_{OC} follows a logarithmic dependence, which is in consistent with the photovoltaic effect observed for the WSe_2 device [21]. Figure 3(d) gives the power generated by the p–n diode with respect to the light density. FF increases from 30.8% to 38.1% with a decrease in light density (shown in Fig. S3(b) in the ESM). I_{SC} and V_{OC} values for the Sample2 under 1,000 nm illumination are ~0.2 μA and 50 mV, respectively, which are decreased with a decrease in the light wavelength. A similar trend is observed as that obtained with changes in the light density, as the photoconductivity dominated the transport properties, as shown in Fig. S3(c) in the ESM. The dependence of the photovoltage and photocurrent on density and wavelength were examined for more devices, and the results are given in Fig. S4 (in the ESM).

As a control experiment, we measured the *I*–*V* curves of a Bi_2Te_3 film and Si substrate under dark and illumination conditions to compare the corresponding results obtained for the n-Bi_2Te_3/p-Si junctions (Fig. S5 in the ESM). The *I*–*V* curves of the Bi_2Te_3 film show little changes under light illumination whereas the Si substrate exhibits a decrease in resistance due to the photoconductivity effect. These results indicate that the photoconductive effects of the Bi_2Te_3 film and Si substrate do not affect the *I*–*V* characteristics of the n-Bi_2Te_3/p-Si junctions.

The photovoltage and photocurrent of the n-Bi_2Te_3/p-Si junction device can be rapidly switched between the on and off modes while the light source is turned on and off under different light densities and wavelengths, as shown in Fig. 4 and Fig. S6 in the ESM (the data were recorded at a sampling rate of 5 data points/s). A steady photovoltage of ~230 mV and a photocurrent of ~0.9 μA can be achieved under NIR illumination (λ = 1,000 nm) upon subjecting the device to repeated switching (Fig. 4). The response time is limited by the data sampling rate, indicating that the device response is faster than 200 ms. The photovoltaic performance of our samples is inferior to that reported for diamond-like amorphous film/Si, carbon nanotubes/Si devices, and graphene/Si [35, 36].

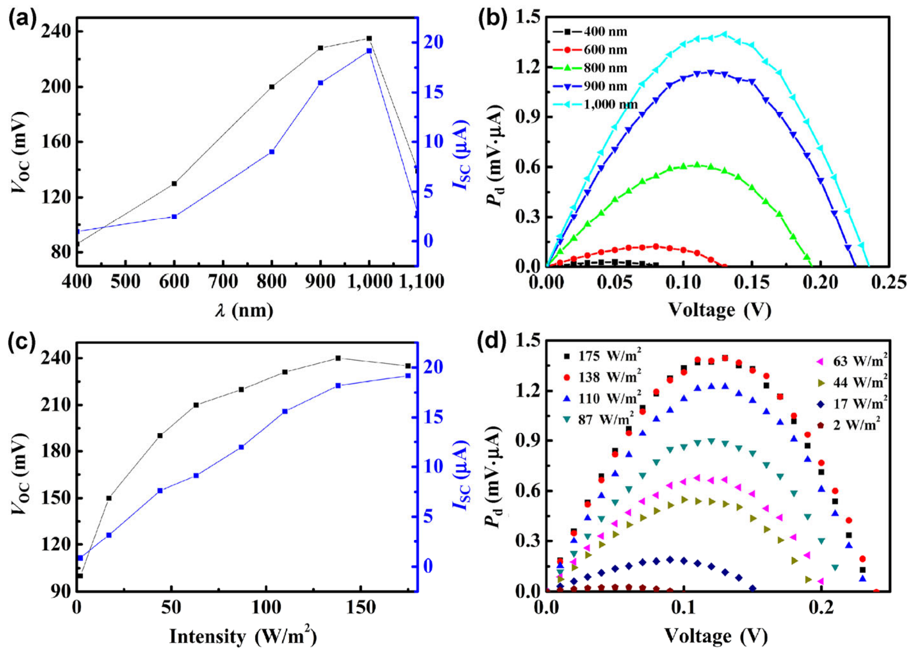

Figure 3 I_{SC} and V_{OC} values of n-Bi_2Te_3/p-Si for Sample1 plotted as a function of (a) wavelength and (c) light density. The power generated by the n-Bi_2Te_3/p-Si diode under illumination with a specific (b) wavelength and (d) density.

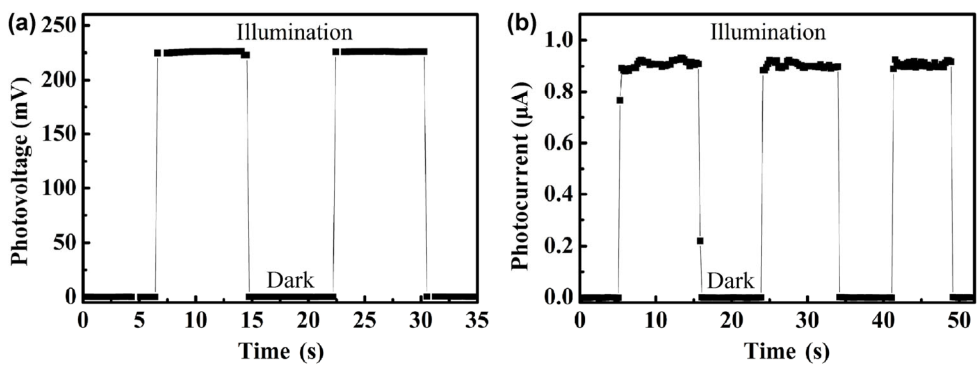

Figure 4 The time trace of (a) photovoltage and (b) photocurrent response of Sample1 measured while turning the light source (λ = 1,000 nm) on and off.

However, the performance might be improved by tuning the conductivity and thickness of Bi_2Te_3 and improving the Bi_2Te_3/p-Si interface.

4 Conclusions

In summary, we fabricated n-Bi_2Te_3/p-Si junctions and characterized the photovoltaic performance of the fabricated devices under dark and light illumination conditions. We examined the photoresponse of the devices for p–n junction solar cell applications. We observed that the photocurrent generation is dominated by the photovoltaic effect in good p–n junctions by measuring the photocurrent (and photovoltage) under light illumination. The best device obtained exhibits an I_{SC} of up to 19.2 μA and a V_{OC} of up to 235 mV under 1,000 nm wavelength with a light intensity about 175 W/m^2, and these values increased with an increase in light intensity. The on–off response time of photocurrent (and photovoltage) under dark and illumination conditions is at least better than 200 ms. We measured the I_{SC} and V_{OC} values of the junctions with different light wavelengths and light intensities. I_{SC} follows a near linear dependence on the light density, whereas V_{OC} follows a logarithmic dependence. The transport properties and photovoltaic effects of the n-Bi_2Te_3/p-Si heterojunctions were affected by the morphology of the Bi_2Te_3 films. This study is important in terms of fundamental understanding and solar cell device applications of TI materials.

Acknowledgements

Z. H. W. acknowledges the National Natural Science Foundation of China (No. 51522104). X. P. A. G. acknowledges the NSF CAREER Award program (No. DMR-1151534) for financial support of research at CWRU. Z. D. Z. acknowledges the National Natural Science Foundation of China (Nos. 51590883, 51331006 and KJZD-EW-M05-3).

Electronic Supplementary Material: Supplementary material (the XRD data of typical Bi_2Te_3 film and the SEM images and photoresponse data of more Bi_2Te_3/Si samples) is is available in the online version of this article at http://dx.doi.org/10.1007/s12274-016-1369-2.

References

[1] Jalali, B.; Fathpour, S. Silicon photonics. *J. Lightwave Technol.* **2006**, *24*, 4600–4615.

[2] Castellanos-Gomez, A.; Poot, M.; Steele, G. A.; van der Zant, H. S. J.; Agrait, N.; Rubio-Bollinger, G. Elastic properties of freely suspended MoS_2 nanosheets. *Adv. Mater*. **2012**, *24*, 772–775.

[3] Radisavljevic, B.; Radenovic, A.; Brivio, J.; Giacometti, V.; Kis, A. Single-layer MoS_2 transistors. *Nat. Nanotechnol*. **2011**, *6*, 147–150.

[4] Mak, K. F.; He, K. L.; Lee, C.; Lee, G. H.; Hone, J.; Heinz, T. F.; Snan, J. Tightly bound trions in monolayer MoS_2. *Nat. Mater*. **2013**, *12*, 207–211.

[5] Sucharitakul, S.; Goble, N. J.; Kumar, U. R.; Sankar, R.; Bogorad, Z. A.; Chou, F. C.; Chen, Y. T.; Gao, X. P. A. Intrinsic electron mobility exceeding 10^3 cm^2/(V·s) in multilayer InSe FETs. *Nano Lett.* **2015**, *15*, 3815–3819.

[6] Xia, F. N.; Mueller, T.; Lin, Y. M.; Valdes-Garcia, A.; Avouris, P. Ultrafast graphene photodetector. *Nat. Nanotechnol*. **2009**, *4*, 839–843.

[7] Lee, H. S.; Min, S. W.; Chang, Y. G.; Park, M. K.; Nam, T.; Kim, H.; Kim, J. H.; Ryu, S.; Im, S. MoS_2 nanosheet phototransistors with thickness-modulated optical energy gap. *Nano Lett*. **2012**, *12*, 3695–3700.

[8] Buscema, M.; Barkelid, M.; Zwiller, V.; van der Zant, H. S. J.; Steele, G. A.; Castellanos-Gomez, A. Large and tunable photo thermoelectric effect in single-layer MoS_2. *Nano Lett*. **2013**, *13*, 358–363.

[9] Novoselov, K. S.; Fal'ko, V. I.; Colombo, L.; Gellert, P. R.; Schwab, M. G.; Kim, K. A roadmap for graphene. *Nature* **2012**, *490*, 192–200.

[10] Wang, Q. H.; Kalantar-Zadeh, K.; Kis, A.; Coleman, J. N.; Strano, M. S. Electronics and optoelectronics of two-dimensional transition metal dichalcogenides. *Nat. Nanotechnol*. **2012**, *7*, 699–712.

[11] Mueller, T.; Xia, F. N.; Avouris, P. Graphene photodetectors for high-speed optical communications. *Nat. Photon*. **2010**, *4*, 297–301.

[12] Xia, F. N.; Mueller, T.; Golizadeh-Mojarad, R.; Freitag, M.; Lin, Y. M.; Tsang, J.; Perebeinos, V.; Avouris, P. Photocurrent imaging and efficient photon detection in a graphene transistor. *Nano Lett*. **2009**, *9*, 1039–1044.

[13] Yin, Z. Y.; Li, H.; Li, H.; Jiang, L.; Shi, Y. M.; Sun, Y. H.; Lu, G.; Zhang, Q.; Chen, X. D.; Zhang, H. Single-layer MoS_2 phototransistors. *ACS Nano* **2012**, *6*, 74–80.

[14] Zhang, W.; Chuu, C. P.; Huang, J. K.; Chen, C. H.; Tsai, M. L.; Chang, Y. H.; Liang, C. T.; Chen, Y. Z.; Chueh, Y. L.; He, J. H. et al. Ultrahigh-gain photodetectors based on

atomically thin graphene-MoS_2 heterostructures. *Sci. Rep.* **2014**, *4*, 3826.

[15] Lee, C. H.; Lee, G. H.; van der Zande, A. M.; Chen, W. C.; Li, Y. L.; Han, M. Y.; Cui, X.; Arefe, G.; Nuckolls, C.; Heinz, T. F. et al. Atomically thin p–n junctions with van der Waals heterointerfaces. *Nat. Nanotechnol*. **2014**, *9*, 676–681.

[16] Li, L. K.; Yu, Y. J.; Ye, G. J.; Ge, Q. Q.; Ou, X. D.; Wu, H.; Feng, D. L.; Chen, X. H.; Zhang, Y. B. Black phosphorus field-effect transistors. *Nat. Nanotechnol*. **2014**, *9*, 372–377.

[17] Deng, Y. X.; Luo, Z.; Conrad, N. J.; Liu, H.; Gong, Y. J.; Najmaei, S.; Ajayan, P. M.; Lou, J.; Xu, X. F.; Ye, P. D. Black phosphorus-monolayer MoS_2 van der Waals heterojunction p–n diode. *ACS Nano* **2014**, *8*, 8292–8299.

[18] Tsai, M. L.; Su, S. H.; Chang, J. K.; Tsai, D. S.; Chen, C. H.; Wu, C. I.; Li, L. J.; Chen, L. J.; He, J. H. Monolayer MoS_2 heterojunction solar cells. *ACS Nano* **2014**, *8*, 8317–8322.

[19] Qiao, H.; Yuan, J.; Xu, Z. Q.; Chen, C. Y.; Lin, S. H.; Wang, Y. S.; Song, J. C.; Liu, Y.; Khan, Q.; Hoh, H. Y. et al. Broadband photodetectors based on graphene-Bi_2Te_3 heterostructure. *ACS Nano* **2015**, *9*, 1886–1894.

[20] Pospischil, A.; Furchi, M. M.; Mueller, T. Solar-energy conversion and light emission in an atomic monolayer p–n diode. *Nat. Nanotechnol*. **2014**, *9*, 257−261.

[21] Groenendijk, D. J.; Buscema, M.; Steele, G. A.; de Vasconcellos, S. M.; Bratschitsch, R.; van der Zant, H. S. J.; Castellanos-Gomez, A. Photovoltaic and photothermoelectric effect in a double-gated WSe_2 device. *Nano Lett*. **2014**, *14*, 5846−5852.

[22] Zhang, H. B.; Zhang, X. J.; Liu, C.; Lee, S. T.; Jie, J. S. High-responsivity, high-detectivity, ultrafast topological insulator Bi_2Se_3/silicon heterostructure broadband photodetectors. *ACS Nano* **2016**, *10*, 5113−5122.

[23] Chen, Y. L.; Analytis, J. G.; Chu, J. H.; Liu, Z. K.; Mo, S. K.; Qi, X. L.; Zhang, H. J.; Lu, D. H.; Dai, X.; Fang, Z. et al. Experimental realization of a three-dimensional topological insulator, Bi_2Te_3. *Science* **2009**, *325*, 178−181.

[24] Wang, K.; Liu, Y. W.; Wang, W. Y.; Meyer, N.; Bao, L. H.; He, L.; Lang, M. R.; Chen, Z. G.; Che, X. Y.; Post, K. et al. High-quality Bi_2Te_3 thin films grown on mica substrates for potential optoelectronic applications. *Appl. Phys. Lett*. **2013**, *103*, 031605.

[25] Fu, L.; Kane, C. L.; Mele, E. J. Topological insulators in three dimensions. *Phys. Rev. Lett*. **2007**, *98*, 106803.

[26] Moore, J. E.; Balents, L. Topological invariants of time-reversal-invariant band structures. *Phys. Rev. B* **2007**, *75*, 121306.

[27] Thomas, G. A.; Rapkine, D. H.; Van Dover, R. B.; Mattheiss, L. F.; Sunder, W. A.; Schneemeyer, L. F.; Waszczak, J. V. Large electronic-density increase on cooling a layered metal: Doped Bi_2Te_3. *Phys. Rev. B* **1992**, *46*, 1553−1556.

[28] Lin, Y. H.; Lin, S. F.; Chi, Y. C.; Wu, C. L.; Cheng, C. H.; Tseng, W. H.; He, J. H.; Wu, C. I.; Lee, C. K.; Lin, G. R. Using n- and p-type Bi_2Te_3 topological insulator nanoparticles to enable controlled femtosecond mode-locking of fiber lasers. *ACS Photonics* **2015**, *2*, 481−490.

[29] Wang, Z. H.; Yang, L.; Li, X. J.; Zhao, X. T.; Wang, H. L.; Zhang, Z. D.; Gao, X. P. A. Granularity controlled nonsaturating linear magnetoresistance in topological insulator Bi_2Te_3 films. *Nano Lett*. **2014**, *14*, 6510−6514.

[30] Wang, Z. H.; Qiu, R. L. J.; Lee, C. H.; Zhang, Z. D.; Gao, X. P. A. Ambipolar surface conduction in ternary topological insulator $Bi_2(Te_{1-x}Se_x)_3$ nanoribbons. *ACS Nano* **2013**, *7*, 2126–2131.

[31] Yao, J. D.; Shao, J. M.; Wang, Y. X.; Zhao, Z. R.; Yang, G. W. Ultra-broadband and high response of the Bi_2Te_3-Si heterojunction and its application as a photodetector at room temperature in harsh working environments. *Nanoscale* **2015**, *7*, 12535–12541.

[32] Haneman, D. Photoelectric emission and work functions of InSb, GaAs, Bi_2Te_3 and germanium. *J. Phys. Chem. Solids* **1959**, *11*, 205–214.

[33] Buscema, M.; Groenendijk, D. J.; Blanter, S. I.; Steele, G. A.; van der Zant, H. S. J.; Castellanos-Gomez, A. Fast and broadband photoresponse of few-layer black phosphorus field-effect transistors. *Nano Lett*. **2014**, *14*, 3347−3352.

[34] Furchi, M. M.; Polyushkin, D. K.; Pospischil, A.; Mueller, T. Mechanisms of photoconductivity in atomically thin MoS_2. *Nano Lett.* **2014**, *14*, 6165−6170.

[35] Mukhopadhyay, K.; Mukhopadhyay, I.; Sharon, M.; Soga, T.; Umeno, M. Carbon photovoltaic cell. *Carbon* **1997**, *35*, 863–864.

[36] Jia, Y.; Wei, J. Q.; Wang, K. L.; Cao, A. Y.; Shu, Q. K.; Gui, X. C.; Zhu, Y. Q.; Zhuang, D. M.; Zhang, G.; Ma, B. B. et al. Nanotube-silicon heterojunction solar cells. *Adv. Mater*. **2008**, *20*, 4594–4598.